Atmospheric Research 233 (2020) 104719

Contents lists available at ScienceDirect

Atmospheric Research

journal homepage: www.elsevier.com/locate/atmosres

High ice concentration observed in tropical maritime stratiform mixed-phase clouds with top temperatures warmer than −8 °C

Jing Yang[a,b,*], Zhien Wang[c,*], Andrew J. Heymsfield[d], Paul J. DeMott[e], Cynthia H. Twohy[f], Kaitlyn J. Suski[g,1], Darin W. Toohey[c]

[a] Collaborative Innovation Center on Forecast and Evaluation of Meteorological Disasters, Key Laboratory for Aerosol-Cloud-Precipitation of China Meteorological Administration, Nanjing University of Information Science and Technology, Nanjing, China
[b] Key Laboratory of Cloud and Fog Physical Environment of China Meteorological Administration, Beijing, China
[c] Department of Atmospheric and Oceanic Sciences, University of Colorado, Boulder, CO, USA
[d] National Center for Atmospheric Research, Boulder, CO, USA
[e] Department of Atmospheric Science, Colorado State University, Fort Collins, CO, USA
[f] NorthWest Research Associates, Redmond, WA, USA
[g] Department of Chemistry and Biochemistry, University of California, San Diego, CA, USA

ARTICLE INFO

Keywords:
High ice concentration
Stratiform cloud
Warm temperature
Aircraft observation
Parcel model simulation

ABSTRACT

In this study, airborne in situ measurements of ice concentrations in mixed-phase clouds over the tropical ocean sampled during the Ice in Clouds Experiment (ICE-T) project are analyzed. High concentrations of ice larger than 250 μm in diameter (0.05–10 L^{-1}) were observed in three *shallow stratiform clouds* whose top temperatures were warmer than −8 °C. The observed ice particles were mostly needles and columns, which are preferred ice crystal shapes between −3 °C and −8 °C. Drizzle size drops (> 100 μm in diameter) were also observed. Biological particles are a potential source of ice nucleating particles (INPs), however, any direct connection to the high ice concentrations observed in the stratiform clouds at temperatures warmer than −8 °C could not be shown, because the observed INP concentrations were 3 orders of magnitude lower than the ice concentrations. Simulations using a parcel model suggest that secondary ice mechanisms, such as the Hallett-Mossop process and fragmentation of freezing drops, which were often assumed previously to be the explanation for observed high ice concentration, cannot fully explain the observed high ice concentration in these shallow stratiform clouds either. The Hallett-Mossop process and fragmentation of freezing drops are important to the strong ice production only in clouds with relatively high concentration of large drops and rimed graupel observed, such as convective clouds. Therefore, other potential ice generation mechanisms, such as droplet collisional freezing and pre-activated INPs, which are still poorly understood, could play significant roles in tropical stratiform and convective mixed-phase clouds.

1. Introduction

Mixed-phase clouds, including stratiform and convective clouds, have a high global coverage between −30 °C and 0 °C (Mazin, 2006; Zhao and Wang, 2010; Jing et al., 2019). Determining the phase (liquid or ice) in mixed-phase clouds is critical to understanding their impacts on the energy budget and climate change (Cantrell and Heymsfield, 2005; Pruppacher and Klett, 2010; Stocker et al., 2014; McFarquhar et al., 2017). The phase partitioning in mixed-phase clouds is strongly related to ice generation, however, ice generation in stratiform mixed-phase clouds at temperatures warmer than −10 °C is not well understood (Mossop and Ono, 1969; Cantrell and Heymsfield, 2005; Zhang et al., 2017) and remains one of the most important sources of uncertainties in numerical models (Fan et al., 2009; Khain et al., 2015; Korolev et al., 2017). Previous studies have suggested that the observed ice concentration in some cases is higher than the typical concentration of ice nucleating particles (INP) at temperatures warmer than −10 °C. However, the possible mechanisms lead to the observed high ice concentration have not been well examined (e.g. Mossop and Ono, 1969; Hobbs and Rangno, 1985; Rangno and Hobbs, 2001).

* Corresponding author at: Collaborative Innovation Center on Forecast and Evaluation of Meteorological Disasters, Key Laboratory for Aerosol-Cloud-Precipitation of China Meteorological Administration, Nanjing University of Information Science and Technology, Nanjing, China.
E-mail addresses: jing.yang@nuist.edu.cn (J. Yang), zhien.wang@colorado.edu (Z. Wang).
[1] Now at Pacific Northwest National Laboratory, Richland, WA, USA.

https://doi.org/10.1016/j.atmosres.2019.104719
Received 21 July 2019; Received in revised form 20 October 2019; Accepted 21 October 2019
Available online 24 October 2019
0169-8095/

Measurements of ice concentrations in stratiform mixed-phase clouds with top temperatures warmer than −10 °C are limited. Using aircraft in situ measurements from five field campaigns, Korolev et al. (2003) showed that most stratiform clouds at mid and high latitudes are dominated by liquid water at temperatures warmer than −10 °C. Hobbs and Rangno (1985) also showed many stratiform clouds with top temperatures warmer than −10 °C were pure liquid at mid and high latitude, but high ice concentration was observed in some cases (0.1–10 L^{-1} in magnitude). Some other previous studies also reported that the ice concentrations observed in stratiform mixed-phase clouds were higher than the typical ice nucleating particle (INP) concentration (Mossop and Ono, 1969; Cooper, 1986; Rangno and Hobbs, 2001). For example, Mossop and Ono (1969) showed that cumulus and stratocumulus, sampled at temperatures warmer than −10 °C over northern New South Wales, contained approximately 10^3 times as many ice particles as expected on the basis of INP concentration measurement. Cooper (1986) showed the ice concentration observed at temperatures warmer than −10 °C in continental mixed-phase clouds varied between 0.01 L^{-1} and 1 L^{-1}, and increased with decreasing temperature. In some Arctic stratiform clouds with top temperatures warmer than −10 °C, the observed ice concentration was higher than 1 L^{-1} (Rangno and Hobbs, 2001), but the mechanisms that lead to the high ice concentrations are not known. Despite the limited measurements of ice concentrations in clouds with top temperatures warmer than −10 °C, the combined CloudSat and CALIPSO measurements confirmed that ice generation in middle level mixed-phase stratiform clouds with top temperatures warmer than −8 °C occurs globally (Zhang et al., 2017).

Primary ice nucleation in mixed-phase stratiform clouds depends on the concentration of INPs. Certain biological particles are known to serve as efficient INPs at temperatures warmer than −12 °C (Möhler et al., 2007; Murray et al., 2012; DeMott et al., 2016; Twohy et al., 2016), and are often implicated as the "seeds" for secondary ice formation. However, observations in cloud-free air suggest the typical INP concentrations are lower than 0.1 L^{-1} at temperatures warmer than −10 °C (Meyers et al., 1992; Murray et al., 2012; Tobo et al., 2013; Petters and Wright, 2015; DeMott et al., 2016, 2017). Therefore, numerical models using primary ice nucleation alone cannot explain or represent the observed high ice concentration in stratiform mixed-phase clouds (Fridlind et al., 2007; Fan et al., 2009; Khain et al., 2015; Yang et al., 2018). Some modelling studies suggest the occurrence of primary ice enhancement mechanisms that are not detected via standard INP measurements, such as the hypothesized production of ice from drop evaporation residuals and drop freezing during evaporation in Arctic stratiform clouds with top temperatures of −15 °C (e.g. Fridlind et al., 2007; Fan et al., 2009). However, there is no evidence that these mechanisms can enhance ice nucleation in warmer stratiform clouds.

There are two known secondary ice production mechanisms that may contribute to ice production at temperatures warmer than −10 °C. The first one is the Hallett-Mossop process (Hallett and Mossop, 1974), which represents the production of ice splinters during riming between −3 °C and −8 °C in mixed-phase clouds. The Hallett-Mossop process is mainly efficient in mature convective clouds, in which large graupel is present (Cardwell et al., 2002; Heymsfield and Willis, 2014). Another secondary ice production process that may be important at temperatures warmer than −10 °C is the fragmentation of freezing drops. Laboratory experiments showed supercooled drops may breakup and produce ice splinters when they freeze, especially when they are nucleated by contacting small ice (Pruppacher and Schlamp, 1975; Wildeman et al., 2017). Lauber et al. (2018) showed the probability of fragmentation for a freezing drop at 300 μm in diameter is approximately 0.36 at −10 °C, and decreases at higher and lower temperatures. Previous studies suggested that fragmentation only applies for freezing drops larger than 50 μm in diameter (Mossop, 1970; Rangno and Hobbs, 2001; Lauber et al., 2018); thus this process is efficient mainly in clouds with relatively high concentration of large drops, such as convective clouds. It is not well understood whether the secondary ice production mechanisms are important or not in the stratiform clouds.

During the ICE in Clouds Experiment - Tropical (ICE-T) project, aircraft measurements were made in various clouds over the Caribbean Sea, most of which were convective clouds at different stages (Heymsfield and Willis, 2014; Yang et al., 2016a,b), while a few were stratiform mixed-phase clouds. The measurements from ICE-T provide a unique dataset to quantitatively estimate the difference in ice concentration between stratiform and convective clouds in the same region. In this study, three *shallow stratiform mixed-phase clouds* cases with top temperatures warmer than −8 °C are shown, the observed high ice concentrations are examined and are compared with the observed total ice concentration in convective clouds sampled during the ICE-T project. The possible contributions of secondary ice production and primary nucleation by biological particles to the strong ice production at temperatures warmer than −8 °C are discussed. The objectives of this study are to provide evidence of the observed high ice concentration in shallow stratiform mixed-phase clouds at warm temperatures over tropical ocean, and to see if the observed high ice concentration can be explained by secondary ice productions or biological INPs. Ice generation in tropical convective and deep stratiform clouds are complicated due to strong coupling of dynamics and microphysical process. The shallow stratiform mixed-phase clouds offer a relatively "simple" environment to study ice generation processes.

The paper is organized as follows: Section 2 describes the dataset and analysis method; Section 3 shows the measurements of ice concentrations in the stratiform mixed-phase clouds sampled during the ICE-T project. Section 4 discusses the possible ice generation mechanisms which may lead to the strong ice production at temperatures warmer than −8 °C. A summary is given in Section 5.

2. Dataset and analysis method

2.1. Measurements

The ICE-T project was conducted from 1 July to 30 July 2011 over the Caribbean Sea, near St. Croix, U.S. Virgin Islands, with the aim of studying the role of ice generation in tropical maritime clouds. The National Center for Atmospheric Research (NCAR) C-130 aircraft was deployed to penetrate convective clouds at different stages of development. Most of the penetrations occurred well below the cloud top, although some were near the cloud top (Heymsfield and Willis, 2014; Yang et al., 2016b). Other than convective clouds, the C-130 also sampled several mixed-phase stratiform clouds. There were 13 research flights in total. During seven of these, the Wyoming Cloud Radar (WCR; Wang et al., 2012) was operated on the C-130 to obtain two-dimensional (2D) reflectivity (Ze) structures, and the Wyoming Cloud Lidar (WCL; Wang et al., 2009) was used to identify liquid-dominated and ice-dominated clouds. The combined radar and lidar measurements can be used to characterize the cloud types (convective or stratiform).

The instruments used to measure the microphysics include a King hot-wire probe, a forward-scattering spectrometer probe (FSSP), a fast 2D cloud (2D-C) probe, a fast 2D precipitation (2D-P) probe, and a counterflow virtual impactor (CVI) probe (Twohy et al., 1997, 2003). The liquid water content (LWC) was measured by the King probe and the drops identified from particle images recorded by the 2D probes. The King probe measures the LWC in droplets smaller than 30 μm in diameter. For drops larger than 30 μm, the King probe underestimates the LWC. 2D probes can provide particle size distribution (PSD) from which the LWC in drops larger than 25 μm in diameter can be estimated. The total LWC is the summation of the LWC measured from the King probe and the drops identified from the 2D probes, minus the overlap between the King and 2D probes (Yang et al., 2016b). To identify ice particles from 2D-C/P particle images, we use the algorithm developed by Yang et al. (2016b), in which ice particles were identified

using the Fourier Transform Technique and the aspect ratios of particle images. Spherical particles were regarded as liquid drops, and non-spherical particles were regarded as ice. This algorithm identifies spherical and non-spherical particles well for particles larger than 10 pixels in diameter (e.g. 250 μm for 2D-C images). In this paper, the diameter of ice is defined as its maximum dimension. The uncertainty of the drop-ice identification for particles larger than 10 pixels in diameter is approximately 10%, which applies mainly for deformed drops and quasi-spherical graupel identification. For needles, columns and other irregular ice particles, the uncertainty is smaller than 10%. The 2D probes were not equipped with anti-shattering tips, so the shattering artifacts on the 2D probes are removed using the technique developed by Field et al. (2006) based on particle interarrival times. This algorithm is originally developed for ice and mixed-phase clouds, and have been used in previous studies of mixed-phase clouds to remove shattering artifacts (e.g. Heymsfield and Willis, 2014). However, it should be noted that this algorithm is not entirely satisfactory, for example, it may remove some small droplets in clouds with high droplet concentration. In this study, we only use the 2D probes for particles with diameters larger than 25 μm, and the ice PSDs are derived only for particles larger than 250 μm. The condensed water content (CWC, liquid plus ice) was measured by the CVI probe. During ICE-T, the CVI reliably measured CWC from about 0.01 $g\,m^{-3}$ to 2.5 $g\,m^{-3}$; Measurements with CWC > 2.5 $g\,m^{-3}$ were not used in this study. For the cases used here, the CVI had a minimum cut-size of 7 μm in diameter, meaning only cloud drops and ice crystals larger than this size have enough inertia to overcome the counterflow and pass into the inlet. Therefore, CWC carried by particles smaller than 7 μm cannot be collected, but most of the CWC is contained in particles larger than 7 μm in sampled ICE-T clouds. The uncertainty of the calculated LWC is 10% compared to the CWC measured by the CVI in pure liquid regions (Yang et al., 2016b).

The INP concentrations were measured in cloud-free air using filter collections for immersion freezing processing in the Colorado State University (CSU) ice spectrometer (IS). During the ICE-T project, filters were mounted on the C-130 and operated at surface sites at 10 m and 1051 m MSL in Puerto Rico (DeMott et al., 2016). For temperatures warmer than −10 °C, the INP were only measured from the coastal site in Puerto Rico and once from the C-130 at the St. Croix airport, thus the measurement may represent not only the marine air, but also the local air above the ground surface (although prevailing winds were typically onshore). On the C-130, the filter collected particles in the cloud-free region within the planetary boundary layer (PBL) at a sample flow rate of 10 volumetric L min^{-1} for 12–40 min at different heights. In Puerto Rico, the filter sampled the particles in the cloud-free region near ground at a sample flow rate of 10 volumetric L min^{-1} as well, but for a much longer time period, which ranged from 4 to 54 h. Collected particles on filters were resuspended in water for distribution into aliquots. The liquid aliquots freeze in the immersion freezing mode as the temperature decreases in a temperature-controlled block, and the freezing process can be monitored. A detailed description of the device and processing can be found in DeMott et al. (2016).

2.2. Parcel model simulations

In this study, cases with high ice concentrations observed in stratiform mixed-phase clouds during ICE-T are examined. In these cases, aircraft penetrations were made about (or less than) 200 m below cloud top, and at approximately −5 °C. The Hallett-Mossop process may contribute substantially to the ice production between −3 °C and − 8 °C (Hallett and Mossop, 1974), especially when riming is significant. Therefore, we performed parcel model simulations with a spectral bin microphysics (SBM) scheme to estimate the secondary ice concentration produced by this process. These simulations help to examine in which cases secondary ice production by this process alone might be significant, and in which cases the Hallett-Mossop process may not explain the observed high ice concentration. The SBM has been applied in the Weather Forecast and Research (WRF) model (Khain et al., 2015). The hydrometeor types in the SBM include liquid drop/rain, ice/snow, and graupel. Each hydrometeor type contains 33 mass bins in its size distribution. The purpose of the simulation is to model the ice production at the flight level at the moment of penetration, so the parcel remains at the constant level. Since the flight level is very close to the cloud top, the modelled ice concentration will not be underestimated with this constraint. The cloud parcel has a depth of 200 m and 50 vertical levels, and the temperature linearly decreases from −5 °C to - 6 °C from the base to top. We also tried a deeper cloud layer (e.g. 400 m) and broader temperature range (e.g. -5 °C to - 7 °C); the simulations provided similar information. The vertical velocity, incoming drop and ice size distributions are from aircraft observations and remain the same during the simulation. These incoming drops and ice interact with each other in the model through the Bergeron process, riming, accretion and aggregation. Primary ice nucleation mechanisms are turned off. The secondary ice particles produced due to the Hallett-Mossop process are constrained in the cloud until they grow larger or are collected by other hydrometeors and fall out. Two simulations were conducted for each case; one with the Hallett-Mossop process turned off, and the other one with the Hallett-Mossop process turned on. Comparison between the two simulations allow us to estimate the ice concentration produced due to the Hallett-Mossop process.

We also use the parcel model simulations to investigate the ice production from the fragmentation of freezing drops. According to previous studies, a supercooled drop larger than 50 μm in diameter may fragment when it contacts small ice (Mossop, 1970; Hobbs and Rangno, 1985; Field et al., 2017). Drops between 50 μm and 300 μm have a relatively high probability (20%–40%) of fragmentation at approximately −15 °C when they freeze (Lauber et al., 2018), and their frequency of fragmentation is lower than 20% at temperatures warmer than −10 °C (Mossop, 1970; Takahashi and Yamashita, 1970; Pander, 2015; Lauber et al., 2018). The secondary ice produced by each fragmented drop is < 2 on average (Brownscombe and Thorndike, 1968; Mossop, 1970). Larger drops, such as millimeter drops, have higher probability of fragmentation than drizzle-size drops (e.g. 100 μm – 300 μm in diameter) at temperatures warmer than −10 °C, and may produce > 2 ice splinters on average (Lauber et al., 2018), but in this study no drops larger than 300 μm were observed in the stratiform clouds. Therefore, in the model simulations, we assume the probability of fragmentation to be 20% for each freezing drop between 50 μm and 300 μm in diameter, and each fragmented drop can produce 2 ice splinters. We also made a sensitivity test assuming each fragmented drop can produce up to 5 ice splinters, as reported by some previous studies (e.g. Lauber et al., 2018), but this will not change the conclusion. The observed drop PSDs and ice concentrations are used as input. The initial size of ice was assumed to be 50 μm in diameter. We also tried smaller sizes of input ice, but the modelled secondary ice concentration was lower than when assuming the input ice crystals were 50 μm in diameter. Here we prefer to present the highest concentration of modelled secondary ice. Two simulations were conducted for each case: one with the fragmentation of freezing drops turned off, and the other one with the fragmentation of freezing drops turned on, the difference in ice concentration between the two simulations is regarded as the contribution from the fragmentation of freezing drops.

3. Observed high ice concentration in stratiform mixed-phase clouds

3.1. Case studies

3.1.1. Environmental conditions

In this study, three penetrations in *shallow stratiform mixed-phase clouds* with top temperatures warmer than −8 °C are shown. In these clouds, the observed ice concentrations were 3–5 orders of magnitude

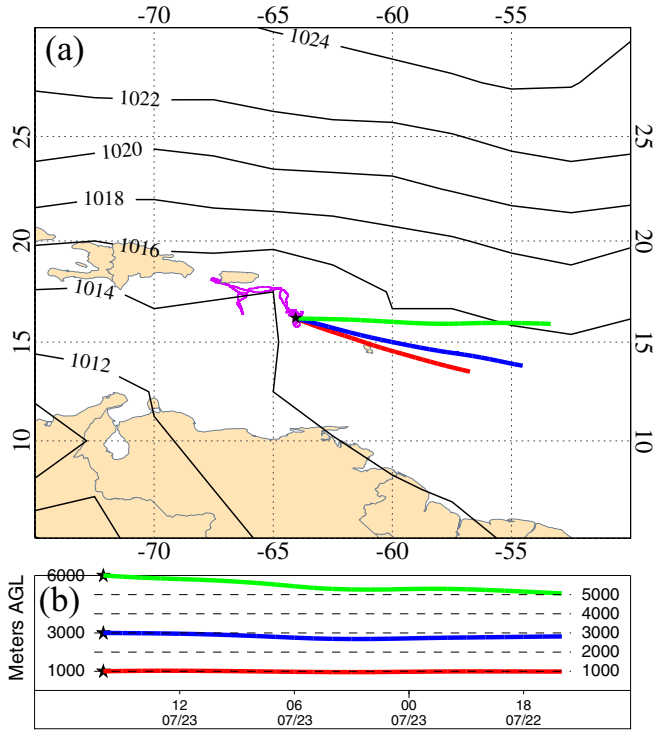

Fig. 1. (a) map of sea level pressure (black), the full flight track on 23 July (purple) and air mass back trajectories at different heights (colored). The sea level pressure is obtained from the 6-hourly NCEP reanalysis data at 12:00 UTC on 23 July. The air mass back trajectories are calculated using the HYSPLIT model based on NCEP reanalysis data, the black star indicates the end point of the air mass trajectories. (b) time series of the vertical variations of the air mass trajectories with the end points at 1000 m, 3000 m, and 6000 m, respectively. (For interpretation of the references to colour in this figure legend, the reader is referred to the web version of this article.)

higher than the measured INP concentration at about −8 °C, which is 10^{-5}–10^{-4} L^{-1} in magnitude (DeMott et al., 2016). All three cases were sampled on 23 July 2011, around 16° N, 64° W, associated with a convective cloud system. An easterly tropical wave was passing through this area in the afternoon. The penetrations were made within 1 h before noon, i.e., before the tropical wave arrived. At the location of interest, the sea level pressure estimated by the NCEP reanalysis data is approximately 1015 mb at 12:00 UTC (8:00 LST) (Fig. 1). The air mass back trajectories derived using the Hybrid Single-Particle Lagrangian Integrated Trajectory model (HYSPLIT) model (Rolph et al., 2017) indicates southeasterly wind at 1 km, and easterly wind at 6 km, consistent with the sounding measurement over Puerto Rico at 12:00 UTC. The wind speed was approximately 10 m s^{-1} at 1 km and 13 m s^{-1} at 6 km. According to the sounding, low level potential instability was observed and the convective available potential energy (CAPE) was approximately 3476 J kg^{-1}. The lifted convection level (LCL) height was approximately 560 m, and the LCL temperature was 24 °C.

During ICE-T, deep convection often occurred in a wide area over the Caribbean Sea, so in the area surrounding stratiform clouds, deep convection was often observed. In order to confirm the stratiform cases shown in this study were neither remnants of old convective clouds nor detrainment from mature convective clouds, images from the Geostationary Operational Environmental Satellite (GOES) were examined. Fig. 2 shows the GOES-13 visible imagery and infrared measurements (indicating cloud top temperature for optically thick clouds) obtained from 13:31:47 to 15:45:18 UTC on 23 July 2011. The red circle in Fig. 2a indicates the location of the mid-level stratiform mixed-phase clouds, whose cloud top temperature was warmer than −10 °C (Fig. 2b). A deep convective cloud was developing upward through the stratiform cloud, and continued to grow with time, with the top temperature of the convective cloud decreasing from −20 °C to −60 °C (Fig. 2a-j). The GOES imagery confirms that the stratiform clouds formed before the deep convection, thus they were neither remnants nor detrainment from old convective clouds. Two penetrations (Case 2 and 3) were made in the stratiform clouds after 15:15:18; Case 1 (Fig. 2k and l) was sampled in a pileus cloud which was not part of the stratiform clouds. From the GOES view, there were high cirrus in the surrounding area of the three cases (Fig. 2i-l). WCR measurement shows that the high cirrus was at ~12 km height and was not seeding the stratiform clouds below.

3.1.2. Case 1

The first case is a pileus cloud, which is a lenticular cloud formed above a convective cloud (Fig. 3). The wave structure of the pileus cloud is evident from the WCL signals (Fig. 3b and c) and the in situ measurements of vertical velocity (Fig. 3e). The updraft was observed above the convective cloud, and the downdraft was observed downwind of the convective cloud. The flight level temperature was warmer than −6 °C (Fig. 3e). Assuming the temperature decreased by 5 °C with increasing height for every 1 km, which is a typical value of moist lapse rate (Minder et al., 2010), the cloud top temperature was approximately −7 °C. The C-130 penetration was made < 200 m below the cloud top. Strong WCR Ze was observed in the convective cloud ~500 m below the flight level (0–20 dBZ), indicating the presence of large particles, while the WCR Ze for the pileus cloud was lower than 0 dBZ (Fig. 3a). The obvious separation of WCR Ze between the pileus and convective cloud observed below the flight level suggests the convection had not penetrated up to the flight level in the pileus cloud. The WCL power varied between 0 dB and 15 dB in the pileus cloud, but was rapidly attenuated in the convective cloud below (Fig. 3b). The strong attenuation is also found for the WCR Ze (Fig. 3a) due to large drops and high liquid water content. The WCL depolarization ratio near the flight level was relatively low in the updraft, suggesting that the updraft in the pileus cloud was dominated by liquid drops (Fig. 3c). The flight level LWC varied between 0 and 0.05 g m^{-3} (Fig. 3d). CVI data were not available for this penetration, but according to the 2D-C measurement, there was no large ice observed in the updraft, supporting the suggestion that the updraft was dominated by liquid water. In the downdraft of the pileus cloud, the WCL depolarization ratio was higher than in the updraft, indicating the presence of non-spherical ice particles. This is supported by the in situ measurements of the concentrations of ice crystals larger than 250 μm in diameter by 2D-C, which varied between 0.05 L^{-1} and 10 L^{-1}, and are higher than the typical INP concentration at −8 °C (10^{-4} L^{-1}) observed over ocean (e.g. DeMott et al., 2016). Similar ice concentrations were also observed in the penetration downwind of the pileus cloud between 15:40:20 and 15:40:40 UTC.

Examples of particle images measured by the 2D-C in the pileus cloud are shown in Fig. 3f. We separate them to three segments according to different penetrations and different ice particle shapes. As noted by the figure, most of the ice particles are needles and columns, some are frozen drops and irregular ice particles (Segment 3). Needles and columns are typical ice crystal shapes that formed through vapor diffusional growth between −5 °C and − 8 °C (Takahashi et al., 1991; Zhang et al., 2014). It takes approximately 10 (20) minutes for an ice particle to grow from 8 μm to 500 (1000) μm in diameter through vapor diffusion (Takahashi et al., 1991; Zhang et al., 2014). Drizzle-size drops (> 100 μm in diameter) were also observed in this case. The drops measured by the FSSP and 2D-C on the C-130 ranged from ~4 μm to ~250 μm, and the ice identified from 2D-C images ranged from ~250 μm to ~1050 μm (Fig. 4). The Hallett-Mossop secondary ice production mechanism cannot explain the observed high ice concentration, because there was no significant riming occurring (Fig. 3f), which is required for the secondary ice generation through this process (Hallett and Mossop, 1974). This is also evident from model simulation

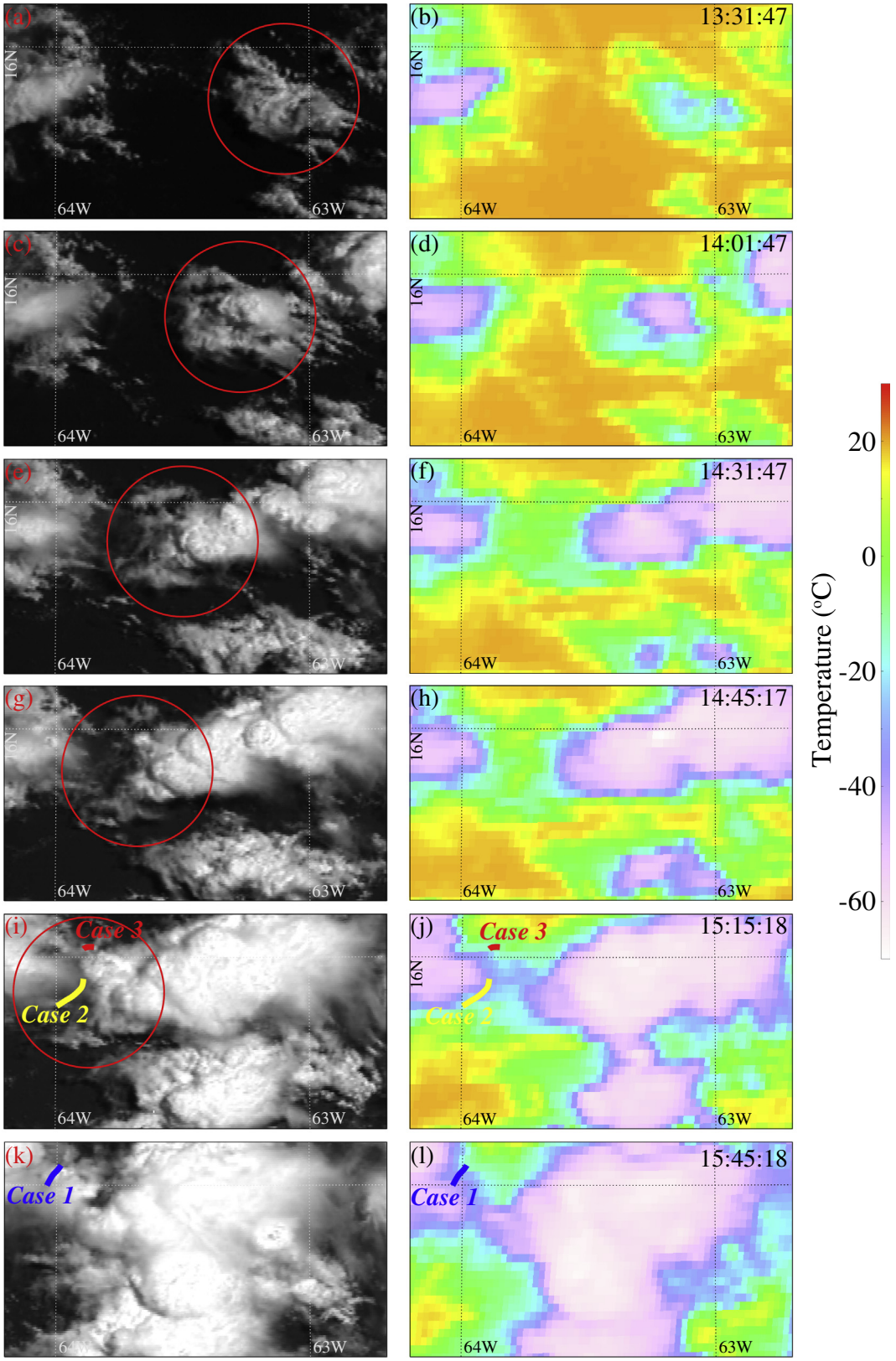

Fig. 2. GOES-13 visible (left panels) imagery and cloud top temperature derived from infrared measurement (right panels). The red circles indicate the location of stratiform clouds, in which deep convection formed and was continuously growing. Three penetrations in stratiform clouds are shown in (i-l). (For interpretation of the references to colour in this figure legend, the reader is referred to the web version of this article.)

(shown later).

3.1.3. Case 2

The second case is an altocumulus (Fig. 5). There was a deep convective cloud nearby, but this cloud was not detrained from the

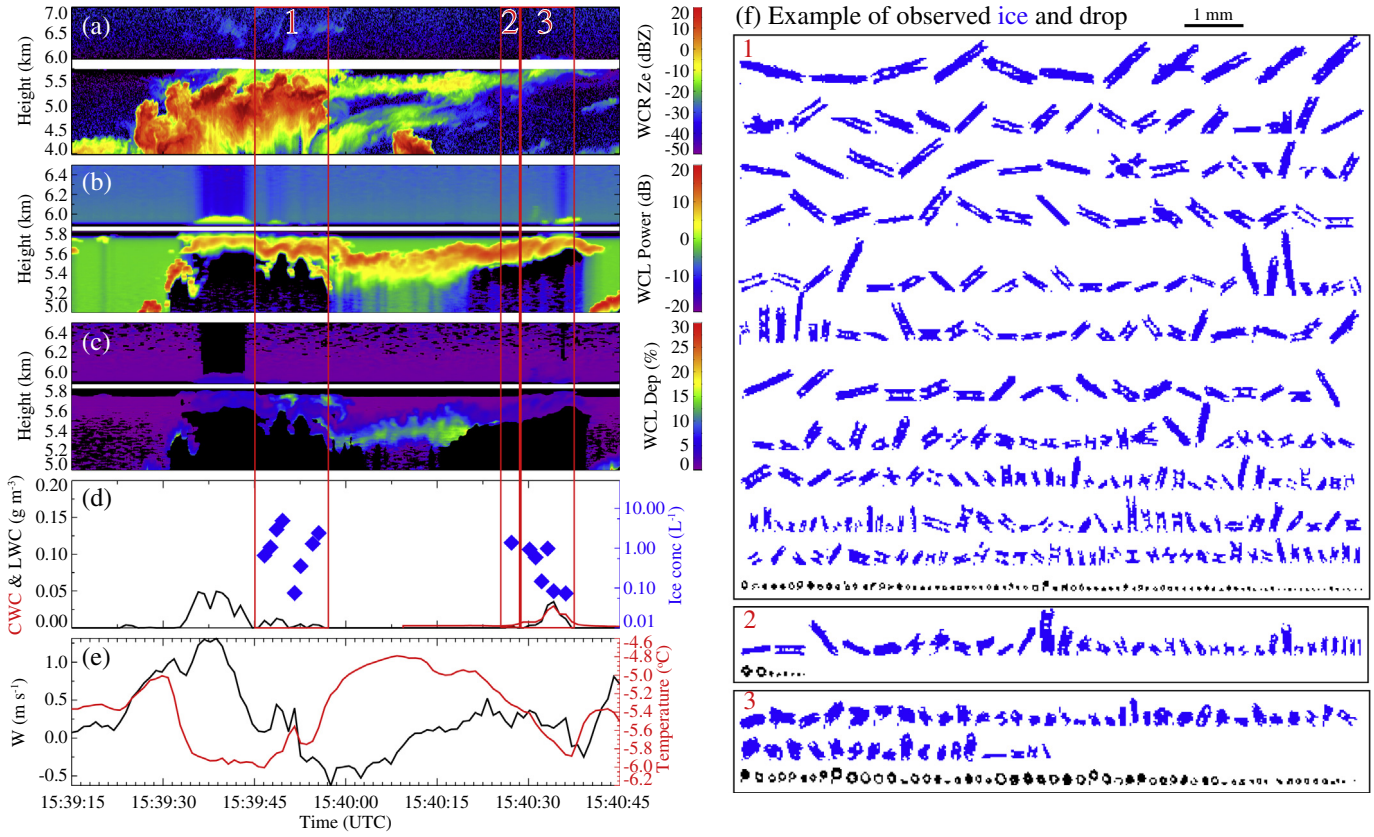

Fig. 3. C-130 penetration through a pileus cloud on July 23, 2011. (a) WCR reflectivity (Ze), (b) WCL power, (c) WCL depolarization ratio, (d) flight level CWC measured by the CVI, LWC measured by the King probe and drops identified from 2D particle images, and concentration of ice larger than 250 μm in diameter measured by 2D probes, (e) flight level vertical velocity and temperature, and (f) examples of drop (black) and ice (blue) images from 2D-C measurements in different segments of the cloud, as indicated by the red boxes in (a)-(d). (For interpretation of the references to colour in this figure legend, the reader is referred to the web version of this article.)

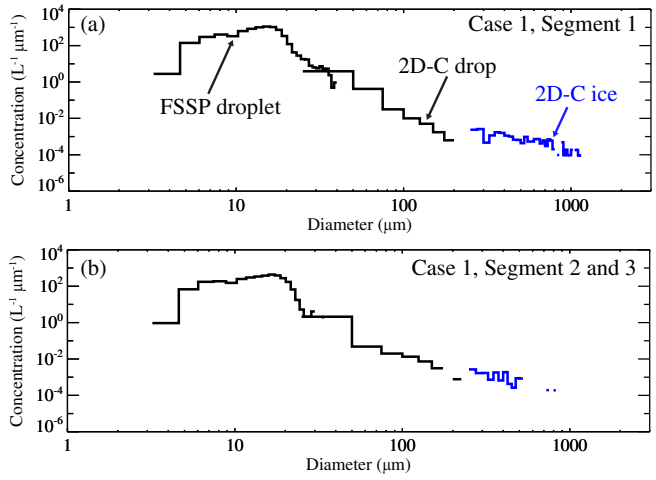

Fig. 4. Drop and ice PSDs observed by FSSP and 2D-C in Case 1, (a) Segment 1, and (b) Segment 2 and 3.

convective cloud (Fig. 2). As indicated by the WCL power (Fig. 5b), the C-130 flew between the mixed-phase layer and the ice virga layer before 15:19:45 UTC, and through the mixed-phase layer after 15:19:45 UTC. The WCR Ze was weaker than −5 dBZ in the mixed-phase layer (Fig. 5a). The WCL depolarization ratio in the mixed-phase layer was low, suggesting it was dominated by liquid drops. A larger WCL depolarization ratio was observed in the ice virga layer, suggesting the initial ice crystals were primarily small, then grew through vapor diffusion, riming or (and) coalescence, and fell out of the mixed-phase layer (Fig. 5c). The flight level updraft velocity varied between $-0.5\,m\,s^{-1}$ and $0.8\,m\,s^{-1}$, and was rather turbulent. The flight level temperature varied between −6.1 °C and − 5.7 °C, and the cloud top temperature was approximately −8 °C (Fig. 5e). The deep convective cloud had high ice concentration and high CWC, and possibly could have affected the edge of the stratiform cloud, so we focus on the penetration before 15:20:00 to avoid the influence of the convective cloud. The flight level LWC and CWC were lower than $0.2\,g\,m^{-3}$ in the stratiform cloud. The concentration of ice larger than 250 μm in diameter varied between $0.05\,L^{-1}$ and $5\,L^{-1}$ (Fig. 5d), which is similar to that observed in the pileus cloud shown in Fig. 3, and higher than the typical INP concentration at such warm temperature. The particle images (Fig. 5f) measured by the 2D-C indicate the ice were mostly needles and columns, some rimed graupel and ice aggregates were also seen in Segment 2, in which cloud top was higher than that in Segment 1 (Fig. 5b). The observed drops ranged from ~4 μm to ~250 μm, and the ice identified from 2D-C images ranged from ~250 μm to ~850 μm, as seen from the PSDs in Fig. 6.

3.1.4. Case 3

The third case is also an altocumulus (Fig. 7) but with different dynamical structures than the second case. The C-130 penetrated through three altocumulus cloud cells, two with weak updrafts (Segment 1 and 2), in which the peak vertical velocities were lower than $1\,m\,s^{-1}$. The third cloud had a relatively strong updraft (Segment 4), in which the peak vertical velocity was approximately $1.5\,m\,s^{-1}$ (Fig. 7d). These altocumulus cells were not the remnants of old convective cloud because these clouds were dominated by liquid water, and according to

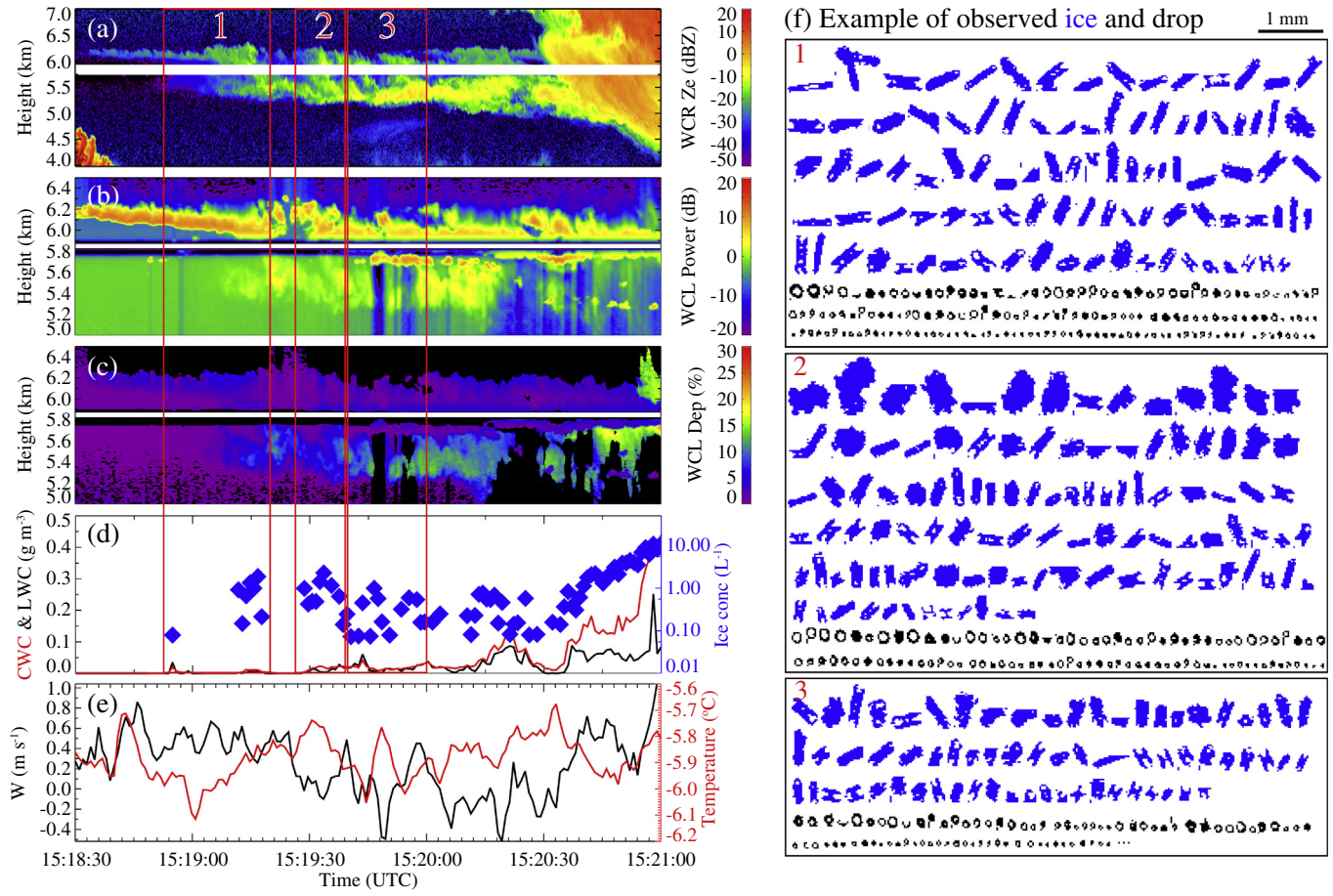

Fig. 5. Same as Fig. 3, but for an altocumulus.

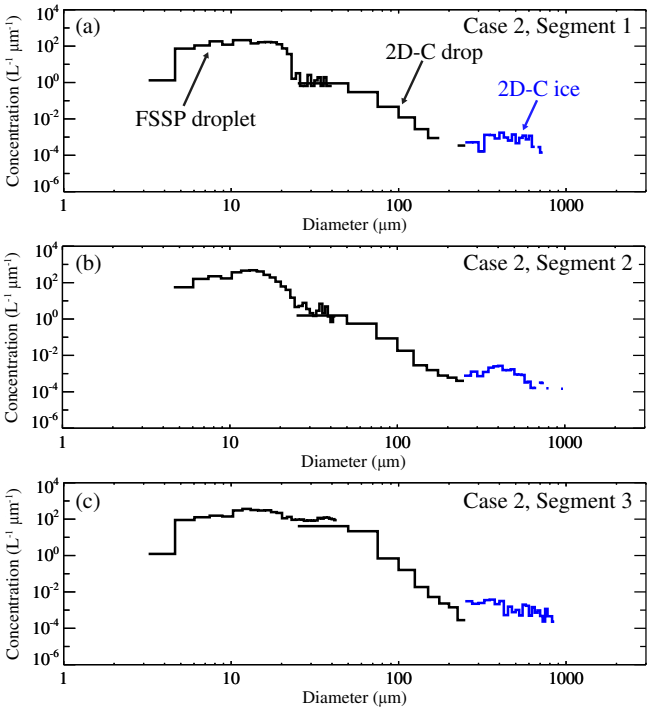

Fig. 6. Same as Fig. 4, but for Case 2.

the satellite images (Fig. 2), there was no deep convective cloud at this location before the altocumulus formed. Particle images measured by the 2D-C suggest there were some rimed graupel (Fig. 7f). Drop and ice PSDs shown in Fig. 8c indicate there were drops larger than 300 μm and ice larger than 1 mm in diameter observed in the relatively strong altocumulus cell (Segment 4), so there might be secondary ice via rime-splintering produced. The secondary ice production is more significant in convective clouds than that in stratiform clouds due to the existence of millimeter drops and more graupel, as indicated by the PSDs shown in Fig. 8d. This suggestion is evident from the model simulations (shown later). Here, the observed PSDs in convective clouds are from the penetrations through convective updrafts with vertical velocity > 1 m s^{-1} (Yang et al., 2016b). In the weakest altocumulus cell (Segment 1), the observed drops were small, which ranged from ~5 μm to ~100 μm in diameter, no ice were observed (Fig. 7f and a), and the WCR Ze was lower than −5 dBZ. For the second altocumulus cell (Segment 2), the WCR Ze varied between −10 dBZ and 5 dBZ, which was higher than that observed in the weakest altocumulus cell. The WCL signals indicate the cloud was dominated by liquid drops, as seen from the relatively large WCL power (Fig. 7b) and low WCL depolarization ratio (Fig. 7c). This is evident from the flight level LWC and CWC, which varied between 0 g m^{-3} and 0.4 g m^{-3} (Fig. 7d). The flight level temperature was approximately −6 °C and the cloud top temperature was approximately −7 °C (Fig. 7e). The concentration of ice larger than 250 μm in diameter varied between 0.1 L^{-1} and 5 L^{-1}. The particles images measured by the 2D-C indicate that the ice crystals were all needles and columns (Fig. 7f), and PSD measurements indicate the drops ranged from ~4 μm to ~300 μm in diameter, and the ice ranged from ~250 μm to ~800 μm in diameter (Fig. 8b).

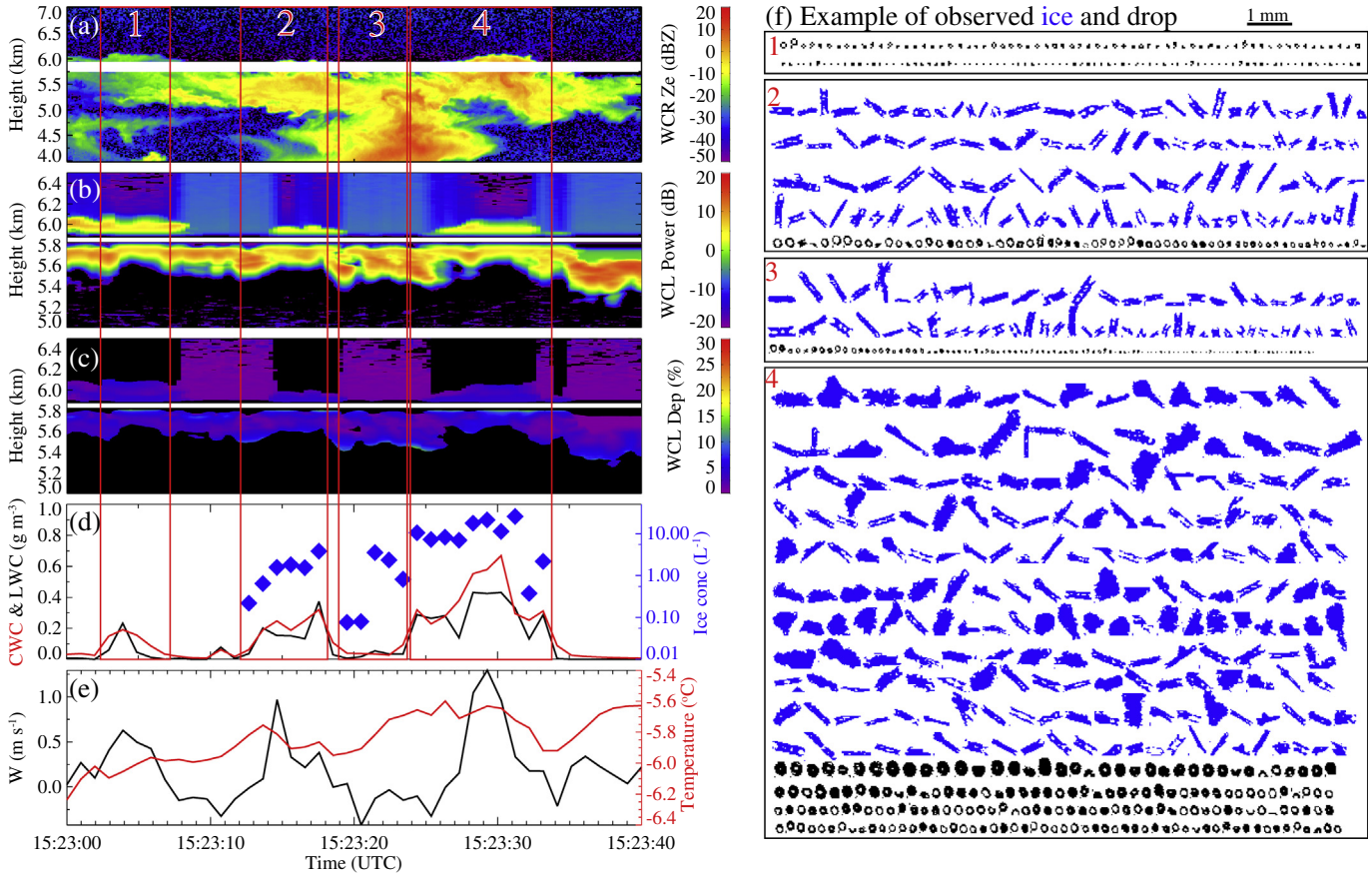

Fig. 7. Same as Fig. 3, but for an altocumulus.

3.2. Comparison of ice concentration between stratiform and convective clouds

The three *shallow stratiform cases* shown above provide evidence that high ice concentrations may form in clouds with top temperatures warmer than −8 °C. The observed ice concentrations are higher than the typical INP concentration at about −8 °C over the ocean (DeMott et al., 2016), but lower than the ice concentration observed in convective clouds. Fig. 9 shows profiles of the concentration of ice larger than 250 μm in diameter observed in convective updrafts from the penetrations < 500 m below cloud top, and in the convective updrafts from the penetrations > 500 m below cloud top, as well as in the three stratiform cases discussed above. A convective updraft is defined as an ascending cloud parcel with vertical velocity continuously $\geq 1\ m\ s^{-1}$ for at least 500 m (LeMone and Zipser, 1980; Yang et al., 2016a). The data are from 7 research flights in which WCR was working properly, because WCR measurements are needed to estimate cloud top height. As seen from the figure, on average, the concentration of ice larger than 250 μm in diameter in the convective updrafts generally increased with decreasing temperature, and were about 6–9 times higher than that in the three stratiform cases at the same temperature range. The maximum concentration of ice larger than 250 μm in diameter was higher than $100\ L^{-1}$, which is in part due to the strong secondary ice production and liquid-ice interaction in the convective clouds. In the convective updrafts near cloud top, a potential secondary ice production mechanism is the fragmentation of freezing drops (Dye and Hobbs, 1968; Field et al., 2017). The Hallett-Mossop process may be less efficient in areas where riming is insignificant (Cooper, 1986; Cardwell et al., 2002), but is certainly vital for convective updrafts where significant riming occurs (Heymsfield and Willis, 2014; Lasher-Trapp et al., 2016; Yang et al., 2016b). Ice-ice collision may also produce ice fragments and enhance the ice generation, but it is efficient mainly at relatively cold temperatures (about −15 °C, Takahashi et al., 1995).

4. Discussion

4.1. Biological particles as possible INPs

Among various species of INPs in the atmosphere, biological aerosols are the leading candidate that can lead to primary ice nucleation at temperatures warmer than −8 °C (Möhler et al., 2007; Pratt et al., 2009; Hoose et al., 2010; Murray et al., 2012). In cloud-free air without large scale uplift or deep convection, biological particles are present mostly within the PBL (Twohy et al., 2016), but during ICE-T, deep convection was occurring widely over the study area, so biological particles could be transported from the PBL to higher levels. Thus, biological INPs that did not rainout with precipitation might contribute to the ice initiation in stratiform clouds.

Fig. 10 compares the concentration of ice larger than 250 μm in diameter measured in the three cases with the temperature-dependent INP concentration measured in ICE-T (the whole dataset). The result from a laboratory experiment during which sea spray aerosols were produced in a marine aerosols reference tank (MART) and phytoplankton blooms took place is also shown in Fig. 10. These data and their detailed descriptions are available in DeMott et al. (2016). As seen from the figure, the INP concentration increases with decreasing temperature, and the observed INP concentration at temperature warmer than −10 °C was lower than $\sim 0.001\ L^{-1}$. With the occurrence of phytoplankton blooms, the INP concentration measured in one laboratory experiment for comparable sea spray aerosol concentrations aligned with the upper bound of field campaign INP concentrations at temperatures warmer than −12 °C, and exceeded INP concentrations at

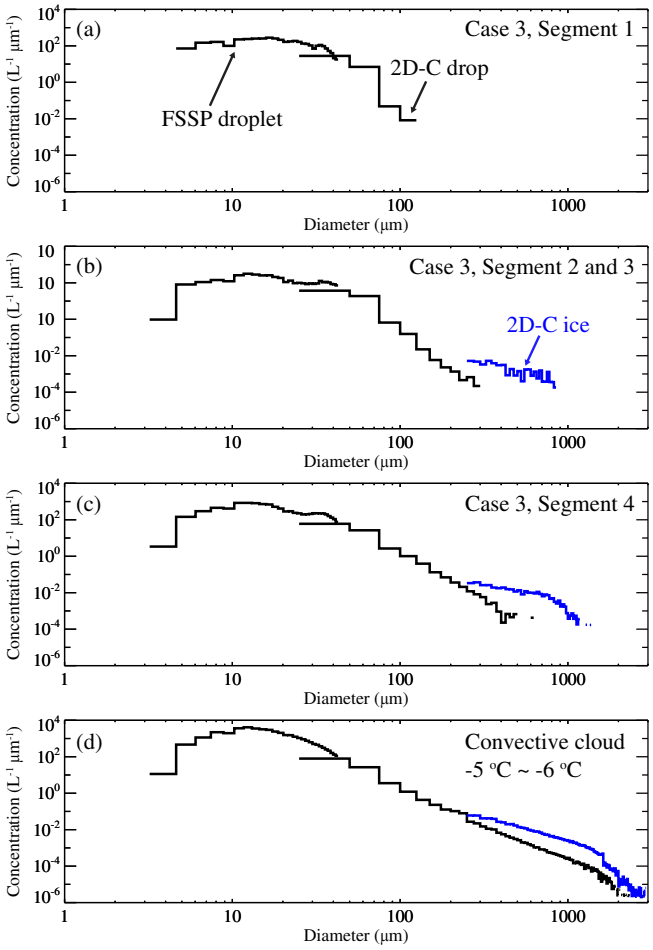

Fig. 8. Same as Fig. 4, but for (a-c) Case 3, and (d) convective updrafts between −5 °C and − 6 °C.

−7 °C by more than an order of magnitude. This suggests that INPs emanating from marine biological processes and emitted with sea spray particles might contribute to the ice initiation in clouds at temperatures warmer than −12 °C. However, the INP concentrations observed during ICE-T were three orders of magnitude lower than the observed ice concentration in the three stratiform mixed-phase clouds, indicating the observed high ice concentration in these stratiform clouds cannot be fully explained by primary ice nucleation through biological INPs.

4.2. Hallett-Mossop process

The modelled ice concentrations produced due to the Hallett-Mossop process with time are shown in Fig. 11a. The input drop and ice PSDs are from the airborne measurements in Segment 2 and 3 in Case 2, Segment 4 in Case 3, and all the convective updrafts sampled between −5 °C and − 6 °C during ICE-T (Figs. 6 and 8). These penetrations are selected because the Hallett-Mossop process possibly played an important role in the ice production. In the model, the Hallett-Mossop process is assumed to occur during riming of both ice crystals and graupel, this helps to assure the modelled secondary ice concentration is not underestimated. In Fig. 11, the solid curves represent the simulations using the observed ice PSDs as the input primary ice, while the dashed curves represent that the input ice PSDs are scaled to a total ice concentration of 0.001 L^{-1}, which is the highest order of the average INP concentration observed at about −8 °C during ICE-T. As seen from the figure, the secondary ice concentration first increases, then remains constant with time, because new secondary ice keeps forming, while older ice particles grow larger and fall out. When using the observed ice

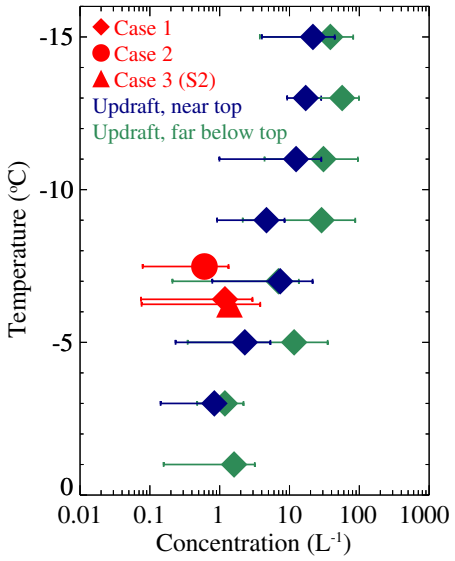

Fig. 9. Profiles of concentration of ice larger than 250 μm in diameter measured by 2D probes in the three stratiform mixed-phase cases (Case 1, 2, and Segment 2 in Case 3), and in the convective updrafts from the penetrations < 500 m below cloud top (blue), as well as in the convective updrafts from the penetrations > 500 m below cloud top (green). The symbols and error bars represent the mean, and 10th - 90th percentile values. The temperature is cloud top temperature for the three stratiform cases, and flight level temperature for the convective clouds. (For interpretation of the references to colour in this figure legend, the reader is referred to the web version of this article.)

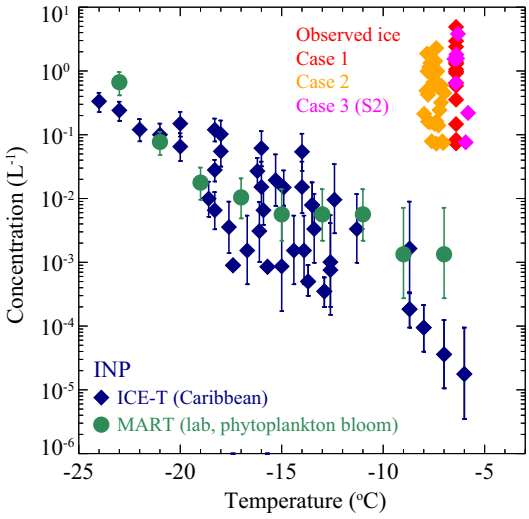

Fig. 10. Concentration of ice larger than 250 μm in diameter measured by 2D probes in Case 1, Case 2, and Case 3 (Segment 2) as a function of cloud top temperature, and temperature-dependent INP concentration measured during ICE-T (blue), and from a laboratory experiment in which phytoplankton bloom took place (green). The symbols for the ice concentration indicate 1-s measurement, and the symbols and error bars for the INP concentration represent the mean and 95%-confidence values.(The result of INP measurements in ICE-T is reproduced from Fig. 1 in Lasher-Trapp et al. (2016) with the copyright permission from American Meteorological Society) (For interpretation of the references to colour in this figure legend, the reader is referred to the web version of this article.)

PSDs as the inputs, for Case 2, the modelled ice concentration produced due to the Hallett-Mossop process is < 0.006 L^{-1}, which is much lower than the observed ice concentration (Fig. 5). Therefore, the Hallett-Mossop process may have contributed to the ice generation, but cannot

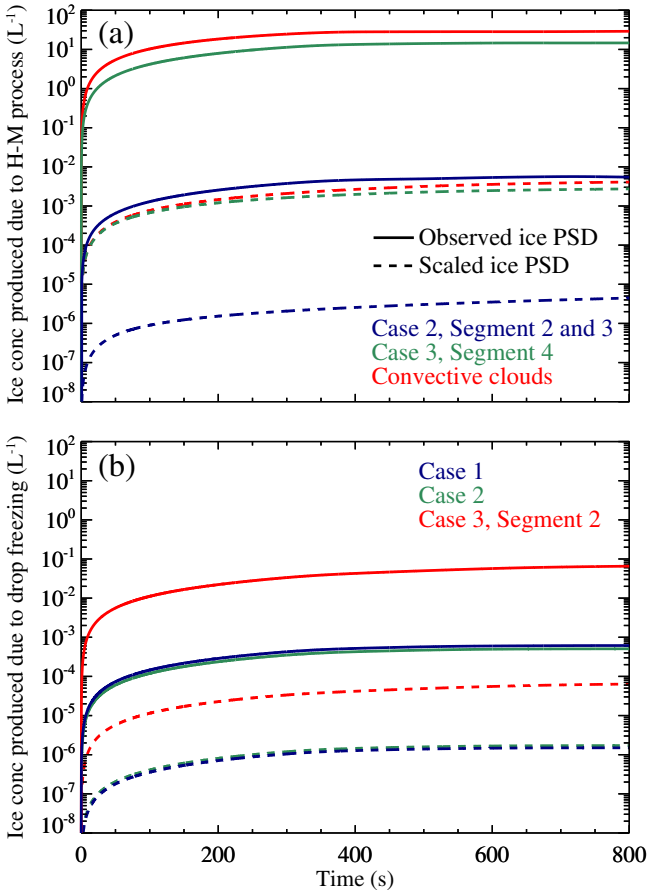

Fig. 11. Ice concentration produced due to (a) Hallett-Mossop process, and (b) fragmentation of freezing drops as a function of time from model simulations. The blue, green and red solid curves represent the simulations using the observed drop and ice PSDs from different cases, and the convective updrafts. The dashed curves are similar to the solid curves, but the ice PSDs are scaled to a total ice concentration of 0.001 L^{-1}, which is the maximum value possible on the basis of INP concentration measurements in ICE-T at −8 °C. (For interpretation of the references to colour in this figure legend, the reader is referred to the web version of this article.)

fully explain the observed high ice concentration. This is consistent with the observation, which suggests the Hallett-Mossop process is not significant in the stratiform clouds without strong updraft. For Segment 4 in Case 3, which had a relatively strong updraft, the modelled ice concentration due to Hallett-Mossop process is as high as 15 L^{-1}, suggesting strong secondary ice production in this case. For the convective updrafts, the modelled ice concentration due to Hallett-Mossop process is as high as 25 L^{-1}. When the input ice concentrations are scaled to 0.001 L^{-1}, the modelled secondary ice concentrations are much less than that modelled using observed ice size distributions due to less significant riming.

4.3. Fragmentation of freezing drops

Drizzle-size drops (> 100 μm in diameter) were observed in the three stratiform cases shown above. Previous studies suggest supercooled drops larger than 50 μm in diameter may fragment and produce ice splinters when they contact small ice (Mossop, 1970; Rangno and Hobbs, 2001; Lauber et al., 2018). Fig. 11b shows the secondary ice concentration produced due to fragmentation of freezing supercooled drops larger than 50 μm in diameter from the model simulations. When using the observed ice concentration as input, the secondary ice concentrations produced due to drop freezing in Case 1 and 2 are lower than 10^{-3} L^{-1}, suggesting the fragmentation of freezing drops cannot fully explain the strong ice generation, consistent with the airborne observation. Here, the number of ice splinters produced by each fragmented drop is assumed to be 2, if assuming a fragmented drop can produce 5 ice splinters, the modelled secondary ice concentration is approximately 2×10^{-3} L^{-1}, which is still much lower than the observed ice concentration. In Segment 2 of Case 3, there were more drizzle-size drops than in Case 1 and 2, so the modelled secondary ice concentration produced due to drop fragmentation is approximately 0.07 L^{-1}, indicating fragmentation of freezing drops at least in part contributed to the ice generation in this case. In Segment 4 of Case 3 and convective clouds, there were more drops larger than 50 μm (Fig. 8c and d), so the modelled secondary ice concentration due to the fragmentation of freezing drops is higher than 2 L^{-1} (not shown). Therefore, both the Hallett-Mossop process and the fragmentation of freezing drops contributed to the ice production in Segment 4 of Case 3 and in convective clouds. When the input ice concentrations are scaled to 0.001 L^{-1}, the modelled secondary ice concentrations from drop freezing are more than two orders of magnitude lower than that modelled using the observed PSDs because of less significant interactions between drops and ice.

4.4. Other ice generation mechanisms

According to the analysis above, the primary ice nucleation through INPs, as well as the Hallett-Mossop process and fragmentation of the drizzle-size drops cannot fully explain the observed high ice concentration in the stratiform clouds shown in this study. There are two other mechanisms, which are currently unmeasurable, that might contribute to the ice generation in stratiform clouds at temperatures warmer than −8 °C.

Previous studies suggested pre-activated INP could be important to ice nucleation at temperatures as warm as −5 °C (e.g. Roberts and Hallett, 1968; Mossop, 1970; Higuchi and Wushiki, 1970). Roberts and Hallett (1968) found that a variety of mineral particles upon which ice has once grown at a low temperature and subsequently evaporated, can retain embryonic ice and grow again at relatively warmer temperature. The ice enhancement by pre-activated kaolinite could be as high as 10^3 at about −10 °C. Higuchi and Wushiki (1970) confirmed pre-activated INP exist in the Arctic and over Mountain Fuji, but not always. During ICE-T, pre-activated INPs, which were from evaporated ice particles falling from higher levels, might exist in the ambient air. According to Fig. 2, the altocumulus sampled in this study had lasted for > 45 min. No precipitation was occurring above the parts which were sampled by the C-130 aircraft, so if there were pre-activated INPs, they were probably long-lived in the ambient air, and could be entrained into the cloud. The INP concentrations at temperatures warmer than −10 °C shown in Fig. 10 do not include pre-activated INPs, because the measurements were made from air sampled at ambient temperatures exceeding 0 °C that would destroy pre-activation (Mossop, 1970). We may note that no system of sampling from aircraft inlets, even into real-time INP instruments, can presently reliably capture pre-activated INPs because of the heating and drying of particles when sampled into inlets and subsequent transfer of air through tubing to instruments at aircraft cabin temperatures.

Another possible ice nucleation mechanism is drop freezing induced by collision between drops (Alkezweeny, 1969; Czys, 1989). This drop collisional freezing mechanism was first noticed by Hobbs (1965), who postulated that collision between supercooled drops may lead to spontaneous freezing. Alkezweeny (1969) confirmed that collision can enhance the probability of freezing for supercooled drops, and provided more evidence of drop collisional freezing from aircraft measurements in cumulus clouds. However, the potential impact of drop collisional freezing on the ice production in cloud is not quantitatively demonstrated. One of the typical shapes of the ice formed through drop collisional freezing is a pair of frozen drops (Alkezweeny, 1969). We do

observe particles consistent with the shape of paired drops from collisional freezing, but there were only a few, and there is no direct evidence to demonstrate they were formed due to collisional freezing. Some laboratory studies suggested collision between supercooled drop and sea salt may also lead to drop freezing (e.g. Niehaus and Cantrell, 2015), but this mechanism is difficult to observe in field measurements, and more laboratory experiments and modelling studies are needed to better understand the role it plays in ice generation in mixed-phase clouds.

In short, *the complicated dynamics and microphysics made it difficult to appreciate the physical mechanisms behind the strong ice production in these clouds*, primary ice nucleation, the Hallett-Mossop process and fragmentation of freezing drops *cannot fully explain* the observed high ice concentration, other mechanisms such as the droplet collisional freezing and pre-activated INPs could play important roles in the ice generation in the stratiform clouds over tropical ocean, these processes are still poorly understood and requires more studies in the future.

5. Summary

In this study, the ice concentrations in mixed-phase clouds over tropical ocean observed during the ICE-T project are analyzed. The cloud microphysics were measured using multiple in situ probes mounted on the NCAR C-130 aircraft. The cloud types and vertical structures are characterized using combined WCR and WCL measurements. In three mid-level *shallow stratiform mixed-phase clouds* whose top temperatures were warmer than −8 °C, the observed concentration of ice larger than 250 μm in diameter varied between 0.05 L^{-1} and 10 L^{-1}. These numbers are substantially higher than the INP concentration observed at temperatures warmer than −8 °C. The particle images measured in these clouds suggest that most of the ice particles were needles and columns, which are preferred ice crystal shapes between −3 °C and − 8 °C, and drizzle-size drops (> 100 μm in diameter) were observed.

Biological particles are the leading candidate for primary ice nucleation at temperatures warmer than −8 °C. However, the INP measurements during ICE-T and in a laboratory experiment were 3 orders of magnitude lower than the observed ice concentrations, even under certain phytoplankton bloom conditions, indicating biological INPs cannot fully explain the observed high ice concentration in the stratiform clouds.

The observed ice particle concentrations, shapes and simulations using a parcel model suggest that the Hallett-Mossop secondary ice production process cannot explain the observed high ice concentration in the *shallow stratiform clouds* without significant riming occurring, and the fragmentation of freezing drops larger than 50 μm in diameter cannot fully explain the observed high ice concentration in these clouds either. In cases with relatively high concentration of large drops and rimmed graupel observed, such as the convective clouds, the Hallett-Mossop process, as well as the fragmentation of freezing drops can be important to the ice production. Comparison between the three stratiform cases against the convective clouds sampled during ICE-T show the concentration of ice larger than 250 μm was enhanced by 6–9 times at −7 °C in convective clouds.

This study provides evidence of observed high ice concentration in *shallow stratiform mixed-phase clouds* with top temperatures warmer than −8 °C over tropical oceans, and shows that primary ice nucleation through biological INP cannot *fully* explain the observed high ice concentrations. In addition, according to the aircraft observation and model simulations, secondary ice productions through the Hallett-Mossop and fragmentation of freezing drop processes, which were often assumed previously to be the explanation for the high ice concentration, cannot *fully* explain the high ice concentration observed during ICE-T in the shallow stratiform clouds either. Better understanding of other potential mechanisms leading to high ice concentrations will require more observational and modelling studies, including development of (difficult) observations and parameterizations for ice generation through pre-activated INPs and droplet collisional freezing, these processes may be important to the ice generation not only in stratiform clouds, but also convective clouds.

Declaration of Competing Interest

The authors declare that they have no known competing financial interests or personal relationships that could have appeared to influence the work reported in this paper.

Acknowledgments

This work is supported by the National Natural Science Foundation of China (41905124), Jiangsu Provincial Basic Research Programme (Natural Science Fund BK20190778, BK20190777), Science and Technology Innovation Project for Overseas Students in Nanjing (R2019LZ03), Capacity Building Project of Weather Modification in Northwest China (ZQC-R18211, RYSY201902), and National Science Foundation [Awards AGS-1034858 (to Z.W.), AGS-1408028 (to C.H.T.) and AGS-1036028 (to P.J.D.)]. The lead author was funded by the Startup Foundation for Introducing Talent of NUIST (2018r093). The authors acknowledge the crew of the NCAR C-130 for collecting these data and providing high-quality products. This study benefitted from the comments by Drs. Kimberly Prather and Gavin Cornwell of University of California, San Diego. We appreciate the editor and anonymous reviewers for the constructive comments and suggestions.

References

Alkezweeny, A.J., 1969. Freezing of supercooled water droplets due to collision. J. Appl. Meteorol. 8, 994–995. https://doi.org/10.1175/1520-0450(1969)008<0994:FOSWDD>2.0.CO;2.

Brownscombe, J.L., Thorndike, N.S.C., 1968. Freezing and shattering of water droplets in free fall. Nature 220, 687–689. https://doi.org/10.1038/220687a0.

Cantrell, W., Heymsfield, A., 2005. Production of ice in tropospheric clouds: a review. Bull. Am. Meteorol. Soc. 86, 795–807. https://doi.org/10.1175/BAMS-86-6-795.

Cardwell, J.R., Choularton, T.W., Wilson, D., Kershaw, R., 2002. Use of an explicit model of the microphysics of precipitating stratiform cloud to test a bulk microphysics scheme. Q. J. R. Meteorol. Soc. 128, 573–592. https://doi.org/10.1256/003590002321042108.

Cooper, W.A., 1986. Precipitation enhancement: a scientific challenge: Ice initiation in natural clouds. Meteorol. Monogr. 43, 29–32. https://doi.org/10.1175/0065-9401-21.43.29.

Czys, R.R., 1989. Ice initiation by collision-freezing in warm-based cumuli. J. Appl. Meteorol. 28, 1098–1104. https://doi.org/10.1175/1520-0450(1989)028<1098:IIBCFI>2.0.CO;2.

DeMott, P.J., et al., 2016. Sea spray aerosol as a unique source of ice nucleating particles. Proceedings of the National Academy of Sciences 113, 5797–5803. https://doi.org/10.1073/pnas.1514034112.

DeMott, P.J., et al., 2017. Comparative measurements of ambient atmospheric concentrations of ice nucleating particles using multiple immersion freezing methods and a continuous flow diffusion chamber. Atmospheric Chemistry and Physics 17, 11227–11245. https://doi.org/10.5194/acp-17-11227-2017.

Dye, J.E., Hobbs, P.V., 1968. The influence of environmental parameters on the freezing and fragmentation of suspended water drops. J. Atmos. Sci. 25, 82–96. https://doi.org/10.1175/1520-0469(1968)025<0082:TIOEPO>2.0.CO;2.

Fan, J., Ovtchinnikov, M., Comstock, J.M., McFarlane, S.A., Khain, A., 2009. Ice formation in Arctic mixed-phase clouds: Insights from a 3-D cloud-resolving model with size-resolved aerosol and cloud microphysics. Journal of Geophysical Research: Atmospheres 114, D4. https://doi.org/10.1029/2008JD010782.

Field, P.R., et al., 2017. Ice formation and evolution in clouds and precipitation: measurement and modeling challenges: secondary ice production: current state of the science and recommendations for the future. Meteorological Monographs 58, 7.1–7.20. https://doi.org/10.1175/AMSMONOGRAPHS-D-16-0014.1.

Field, P.R., Heymsfield, A.J., Bansemer, A., 2006. Shattering and particle interarrival times measured by optical array probes in ice clouds. J. Atmos. Ocean. Technol. 23, 1357–1371. https://doi.org/10.1175/JTECH1922.1.

Fridlind, A.M., Ackerman, A.S., McFarquhar, G., Zhang, G., Poellot, M.R., DeMott, P.J., Prenni, A.J., Heymsfield, A.J., 2007. Ice properties of single-layer stratocumulus during the Mixed-Phase Arctic Cloud Experiment: 2. Model results. Journal of Geophysical Research: Atmospheres 112, D24202. https://doi.org/10.1029/2007JD008646.

Hallett, J., Mossop, S.C., 1974. Production of secondary ice particles during the riming process. Nature 249, 26–28. https://doi.org/10.1038/249026a0.

Heymsfield, A.J., Willis, P., 2014. Cloud conditions favoring secondary ice particle

production in tropical maritime convection. J. Atmos. Sci. 71, 4500–4526. https://doi.org/10.1175/JAS-D-14-0093.1.
Higuchi, K., Wushiki, H., 1970. Observations of pre-activated ice nuclei in the atmosphere at subzero temperature. Journal of the Meteorological Society of Japan. Ser. II 48, 250–254. https://doi.org/10.1175/JAS-D-14-0093.1.
Hobbs, P.V., 1965. The aggregation of ice particles in cloud and fogs at low temperature. J. Atmos. Sci. 22, 296–299. https://doi.org/10.1175/1520-0469(1965)022<0296:TAOIPI>2.0.CO;2.
Hobbs, P.V., Rangno, A.L., 1985. Ice particle concentrations in clouds. J. Atmos. Sci. 42, 2523–2549. https://doi.org/10.1175/1520-0469(1985)042<2523:IPCIC>2.0.CO;2.
Hoose, C., Kristjánsson, J.E., Burrows, S.M., 2010. How important is biological ice nucleation in clouds on a global scale? Environ. Res. Lett. 5, 024009. https://doi.org/10.1088/1748-9326/5/2/024009.
Jing, X., Geerts, B., Wang, Y., Liu, C., 2019. Ambient factors controlling the wintertime precipitation distribution across mountain ranges in the interior western united states. Part II: changes in orographic precipitation distribution in a pseudo-global warming simulation. J. Appl. Meteor. Climatol. 58, 695–715. https://doi.org/10.1175/JAMC-D-18-0173.1.
Khain, A.P., et al., 2015. Representation of microphysical processes in cloud-resolving models: Spectral (bin) microphysics versus bulk parameterization. Reviews of Geophysics 53, 247–322. https://doi.org/10.1002/2014RG000468.
Korolev, A., et al., 2017. Ice formation and evolution in clouds and precipitation: measurement and modeling challenges: mixed-phase clouds: progress and challenges. Meteorological Monographs 58, 5.1–5.50. https://doi.org/10.1175/AMSMONOGRAPHS-D-17-0001.1.
Korolev, A.V., Isaac, G.A., Cober, S.G., Strapp, J.W., Hallett, J., 2003. Microphysical characterization of mixed-phase clouds. Q. J. R. Meteorol. Soc. 129, 39–65. https://doi.org/10.1256/qj.01.204.
Lasher-Trapp, S., Leon, D.C., DeMott, P.J., Villanueva-Birriel, C.M., Johnson, A.V., Moser, D.H., Tully, C.S., Wu, W., 2016. A multisensor investigation of rime splintering in tropical maritime cumuli. J. Atmos. Sci. 73, 2547–2564. https://doi.org/10.1175/JAS-D-15-0285.1.
Lauber, A., Kiselev, A., Pander, T., Handmann, P., Leisner, T., 2018. Secondary ice formation during freezing of levitated droplets. J. Atmos. Sci. 75, 2815–2826. https://doi.org/10.1175/JAS-D-18-0052.1.
LeMone, M.A., Zipser, E.J., 1980. Cumulonimbus vertical velocity events in GATE. Part I: Diameter, intensity and mass flux. J. Atmos. Sci. 37, 2444–2457. https://doi.org/10.1175/1520-0469(1980)037<2444:CVVEIG>2.0.CO;2.
Mazin, I.P., 2006. Cloud phase structure: Experimental data analysis and parameterization. J. Atmos. Sci. 63, 667–681. https://doi.org/10.1175/JAS3660.1.
McFarquhar, G.M., Baumgardner, D., Heymsfield, A.J., 2017. Ice formation and evolution in clouds and precipitation: measurement and modeling challenges: background and overview. Meteorological Monographs 58, v–ix. https://doi.org/10.1175/JAS3660.1.
Meyers, M.P., DeMott, P.J., Cotton, W.R., 1992. New primary ice-nucleation parameterizations in an explicit cloud model. J. Appl. Meteorol. 31, 708–721. https://doi.org/10.1175/1520-0450(1992)031<0708:NPINPI>2.0.CO;2.
Minder, J.R., Mote, P.W., Lundquist, J.D., 2010. Surface temperature lapse rates over complex terrain: Lessons from the Cascade Mountains. J. Geophys. Res. Atmos. 115, D14122. https://doi.org/10.1029/2009JD013493.
Möhler, O., DeMott, P.J., Vali, G., Levin, Z., 2007. Microbiology and atmospheric processes: the role of biological particles in cloud physics. Biogeosciences 4, 1059–1071. https://doi.org/10.5194/bg-4-1059-2007.
Mossop, S.C., 1970. Concentrations of ice crystals in clouds. Bull. Am. Meteorol. Soc. 51, 474–479. https://doi.org/10.1175/1520-0477(1970)051<0474:COICIC>2.0.CO;2.
Mossop, S.C., Ono, A., 1969. Measurements of ice crystal concentration in clouds. J. Atmos. Sci. 26, 130–137. https://doi.org/10.1175/1520-0469(1969)026<0130:MOICCI>2.0.CO;2.
Murray, B.J., O'Sullivan, D., Atkinson, J.D., Webb, M.E., 2012. Ice nucleation by particles immersed in supercooled cloud droplets. Chem. Soc. Rev. 41, 6519–6554. https://doi.org/10.1039/C2CS35200A.
Niehaus, J., Cantrell, W., 2015. Contact freezing of water by salts. The Journal of Physical Chemistry Letters 6, 3490–3495. https://doi.org/10.1021/acs.jpclett.5b01531.
Pander, T.J., 2015. Laboratory Ice Multiplication Experiments in Levitated Microdroplets. Doctoral dissertation. University of Heidelberg, Germany (131pp).
Petters, M.D., Wright, T.P., 2015. Revisiting ice nucleation from precipitation samples. Geophys. Res. Lett. 42, 8758–8766. https://doi.org/10.1002/2015GL065733.
Pratt, K.A., DeMott, P.J., French, J.R., Wang, Z., Westphal, D.L., Heymsfield, A.J., Twohy, C.H., Prenni, A.J., Prather, K.A., 2009. In situ detection of biological particles in cloud ice-crystals. Nat. Geosci. 2, 398. https://doi.org/10.1038/ngeo521.
Pruppacher, H.R., Klett, J.D., 2010. Microphysics of clouds and precipitation. Atmospheric and Oceanographic Sciences Library 954.
Pruppacher, H.R., Schlamp, R.J., 1975. A wind tunnel investigation on ice multiplication by freezing of waterdrops falling at terminal velocity in air. J. Geophys. Res. 80, 380–386. https://doi.org/10.1029/JC080i003p00380.
Rangno, A.L., Hobbs, P.V., 2001. Ice particles in stratiform clouds in the Arctic and possible mechanisms for the production of high ice concentrations. J. Geophys. Res. 106, 15065–15075. https://doi.org/10.1029/2000JD900286.
Roberts, P., Hallett, J., 1968. A laboratory study of the ice nucleating properties of some mineral particulates. Q. J. R. Meteorol. Soc. 94, 25–34. https://doi.org/10.1002/qj.49709439904.
Rolph, G., Stein, A., Stunder, B., 2017. Real-time environmental applications and display system: READY. Environ. Model Softw. 95, 210–228. https://doi.org/10.1016/j.envsoft.2017.06.025.
Stocker, T., et al., 2014. Climate change 2013: the physical science basis. In: Working Group I contribution to the Fifth assessment report of the Intergovernmental Panel on Climate Change. Cambridge University Press.
Takahashi, C., Yamashita, A., 1970. Shattering of frozen water drops in a supercooled cloud. Journal of the Meteorological Society of Japan. Ser. II 48, 373–376. https://doi.org/10.2151/jmsj1965.48.4_373.
Takahashi, T., Endoh, T., Wakahama, G., Fukuta, N., 1991. Vapor diffusional growth of free-falling snow crystals between −3 and −23 °C. *J. meteor.* Soc. Japan 69, 15–30. https://doi.org/10.2151/jmsj1965.69.1_15.
Takahashi, T., Nagao, Y., Kushiyama, Y., 1995. Possible high ice particle production during graupel–graupel collisions. J. Atmos. Sci. 52, 4523–4527. https://doi.org/10.1175/1520-0469(1995)052<4523:PHIPPD>2.0.CO;2.
Tobo, Y., Prenni, A.J., DeMott, P.J., Huffman, J.A., McCluskey, C.S., Tian, G., Pöhlker, C., Pöschl, U., Kreidenweis, S.M., 2013. Biological aerosol particles as a key determinant of ice nuclei populations in a forest ecosystem. Journal of Geophysical Research: Atmospheres 118, 10100–10110. https://doi.org/10.1002/jgrd.50801.
Twohy, C.H., et al., 2016. Abundance of fluorescent biological aerosol particles at temperatures conducive to the formation of mixed-phase and cirrus clouds. Atmospheric Chemistry and Physics 16, 8205–8225. https://doi.org/10.5194/acp-16-8205-2016.
Twohy, C.H., Schanot, A.J., Cooper, W.A., 1997. Measurement of condensed water content in liquid and ice clouds using an airborne counterflow virtual impactor. J. Atmos. Ocean. Technol. 14, 197–202. https://doi.org/10.1175/1520-0426(1997)014<0197:MOCWCI>2.0.CO;2.
Twohy, C.H., Strapp, J.W., Wendisch, M., 2003. Performance of a counterflow virtual impactor in the NASA Icing Research Tunnel. J. Atmos. Ocean. Tech. 20, 781–790. https://doi.org/10.1175/1520-0426(2003)020<0781:POACVI>2.0.CO;2.
Wang, Z., et al., 2012. Single aircraft integration of remote sensing and in situ sampling for the study of cloud microphysics and dynamics. Bull. Amer. Meteor. Soc. 93, 653–668. https://doi.org/10.1175/BAMS-D-11-00044.1.
Wang, Z., Wechsler, P., Kuestner, W., French, J., Rodi, A., Glover, B., Burkhart, M., Lukens, D., 2009. Wyoming cloud lidar: Instrument description and applications. Opt. Express 17, 13576–13587. https://doi.org/10.1364/OE.17.013576.
Wildeman, S., Sterl, S., Sun, C., Lohse, D., 2017. Fast dynamics of water droplets freezing from the outside in. Phys. Rev. Lett. 118, 084101. https://doi.org/10.1103/PhysRevLett.118.084101.
Yang, J., Wang, Z., Heymsfield, A., French, J., 2016a. Characteristics of vertical air motion in isolated convective clouds. Atmos. Chem. Phys. 16, 10159–10173. https://doi.org/10.5194/acp-16-10159-2016.
Yang, J., Wang, Z., Heymsfield, A.J., Luo, T., 2016b. Liquid-ice mass partition in tropical maritime convective clouds. J. Atmos. Sci. 73, 4959–4978. https://doi.org/10.1175/JAS-D-15-0145.1.
Yang, J., Wang, Z., Heymsfield, A., 2018. On the freezing time of supercooled drops in developing convective clouds over tropical ocean. Atmos. Res. 211, 30–37. https://doi.org/10.1016/j.atmosres.2018.04.023.
Zhang, D., Wang, Z., Heymsfield, A., Fan, J., Luo, T., 2014. Ice concentration retrieval in stratiform mixed-phase clouds using cloud radar reflectivity measurements and 1D ice growth model simulations. J. Atmos. Sci. 71, 3613–3635. https://doi.org/10.1175/JAS-D-13-0354.1.
Zhang, D., Wang, Z., Luo, T., Yin, Y., Flynn, C., 2017. The occurrence of ice production in slightly supercooled Arctic stratiform clouds as observed by ground-based remote sensors at the ARM NSA site. Journal of Geophysical Research: Atmospheres 122, 2867–2877. https://doi.org/10.1002/2016JD026226.
Zhao, M., Wang, Z., 2010. Comparison of Arctic clouds between European Center for Medium-Range Weather Forecasts simulations and Atmospheric Radiation Measurement climate Research Facility long-term observations at the North Slope of Alaska Barrow site. J. Geophys. Res. 115, D23202. https://doi.org/10.1029/2010JD014285.